IEEE Access
Multidisciplinary | Rapid Review | Open Access Journal

Received December 29, 2020, accepted January 23, 2021, date of publication February 5, 2021, date of current version March 24, 2021.

Digital Object Identifier 10.1109/ACCESS.2021.3057423

Measurement Interface Stiffness of Bonded Structures Using Air-Coupled Ultrasonic Transmission Technology

XINGGUO WANG, JIAXIANG WANG, ZHICHENG HUANG, AND XIAOGAO LI
School of Mechanical and Electronic Engineering, Jingdezhen Ceramic Institute, Jingdezhen 333403, China

Corresponding author: Xingguo Wang (wangxingguo@jci.edu.cn)

This work was supported in part by the National Natural Science Foundation of China under Grant 51565020, Grant 11862007, and Grant 51305184; and in part by the Natural Science Foundation of Jiangxi Province, China, under Grant 20171BAB206032 and Grant 20171ACB21047.

ABSTRACT An air-coupled ultrasonic technology is introduced as a new tool for evaluating the interfacial quality of bonded structures in this paper. Thus, a mathematical model including the stiffness coefficient, the transmission coefficient and the frequency, etc. is proposed. Two type resonant frequencies, namely, the first type resonance frequency (RFI) and the second type resonance frequency (RFII), have been obtained by numerical solving the model. The interval of the RFI is related to the thickness of a polymethyl methacrylate (PMMA) layer. Similarly, the interval of the RFII depends on the thickness of an aluminum (Al) layer. In addition, the stiffness coefficient is associated with the RFI but not with the RFII. The RFI drifts to high-frequency with different speed from the low stiffness coefficient to the high stiffness coefficient, which no longer changes when the stiffness coefficient tends to infinity. The before-RFII moves faster than after-RFI in a ''Period'' of the RFII. With the increase of the stiffness coefficient, the transmission coefficient gradually increases, and then increases slowly when the stiffness coefficient approaches to a critical value. Several double-layer bonded samples with the different thicknesses were made to carry out air-coupled ultrasonic experiment. The change of stiffness coefficients was simulated by different bonding time. Transmission signals from ultrasonic testing were recorded for further processing. Comparing the experimental and simulation results, the stiffness coefficient of the bonded structure can be judged by the RFI and the transmission coefficient.

INDEX TERMS Air-coupled ultrasonic, bonded structure, transmission coefficient, stiffness coefficient, resonant frequency.

I. INTRODUCTION

Laminated composite structures are widely used in aircraft engine shroud and wing spoiler, solid rocket motor casing, missile launcher canister due to its high specific strength, high specific modulus, superior shock absorption, fatigue resistance, and simple manufacture technology [1]–[3]. Thus, research on the acoustic characteristics of sandwich or interface of composite structures has always been the focus of attention, which is used to design the materials and properties of interface layer [4], [5]. Bonded structure is one of the most common forms of composite materials, and its interface failure caused by insufficient stiffness from the bonding layer occurs frequently and even leads to accidents. Therefore, it is necessary to measure and evaluate the interfacial bonding quality of laminated composite structures to reveal the hidden dangers in time and avoid serious consequences [6]. There are many ways to distinguish the quality of the interface bonding, one of which is ultrasonic techniques that have always been favored by inspectors [7], [8]. Ultrasonic technology has no obvious effect on the bonding rigidity of the structure, although it is recognized as an effective defect detection method. In terms of the method of impedance and sound pressure, Rose *et al.* [9] derived the expressions of the reflection coefficients and transmission coefficients of bulk waves in the multilayered homogeneous mediums. Wang [10] studied the acoustic reflection and transmission characteristics of layered solid medium with rigid interface and slip

The associate editor coordinating the review of this manuscript and approving it for publication was Wuliang Yin.

interface by the transfer matrix. The analytical expressions of reflection coefficients and transmission coefficients were deduced according to the incidence mode of P-wave or S-wave. Rokhlin *et al.* [11] regarded the bonding interface as a viscoelastic layer to investigate the bulk wave propagation characteristics of a finite thickness interface layer in a multi-layered adhesive structure between two semi-infinite isotropic mediums. The results reflected that the ideal bonding and debonding interface can be well distinguished. The ''right peak'' drift of the spring model, ignoring the thickness of bonded layer, is obtained. An *et al.* [12] analyzed the low-frequency reflection rules of waves in aluminum-bonded layer-aluminum weak bond structure.

Utilizing ultrasonic guided waves to evaluate the interface quality, Banerjee [13] analyzed the guided wave propagation mode in bonded structures. It shows that the echo in vertical excitation is controlled by the first-order antisymmetric mode. Castaings [14] studied the propagation of the SH wave in aluminum-resin glass-aluminum lap joint structure with different interface bonding quality by finite element and experiment. Yew *et al.* [15] applied the SH wave to evaluate the quality of the bonding layer. It can be concluded that the cutoff frequency of the second-order mode from SH wave in bonded structures mainly depends on the thickness and mechanical properties of the bonding layer. Zhang *et al.* [16] conducted a laser ultrasonic technique with pulse-echo mode to detect the debonding in multilayer bonded structures and proposed a quantitative method to evaluate defect size. Gao and Zeng [17] studied the propagation characteristics of Lamb waves in isotropic composite laminates, and established an improved method for locating the damage of composite structures. Based on the acoustic wave equation and boundary conditions, Liu *et al.* [18] used the potential function to analyze the acoustic propagation mechanism of the layered composites with arbitrary incident angles, and illustrated the variation of the amplitude and phase of the transmission coefficient with the frequency. Ding *et al.* [19] derived the expression of reflection and transmission coefficient of the SH wave in multi-layer plate-like bonded structures in the light of the wave propagation equation and shear stiffness coefficient, which provided a theoretical basis for the SH wave to evaluate multi-layer plate-like bonded structure. Liu *et al.* [20] proposed a way to measure the plane bonded structure using wideband focused ultrasound in vertical direction. The reflection coefficient of the structural plane wave varying with the frequency and the incident angle was acquired by the inversion method, and the performance of bonded structures was evaluated in terms of the reflection coefficient.

From the analysis above, scholars developed many methods combined with ultrasonic bulk waves or guided waves by interface simplification models to illuminate bonded structures and achieved some significant results. Traditional ultrasonic testing requires liquid grease and other substances as couplant for sound waves to propagate from sensors to the measured medium as much as possible, but the couplant may contaminate the surface between of sensors and media even penetrate them to affect the testing results. Consequently, air-coupled ultrasound is getting more and more attention [21], [22].

As early as the 1960s, an air-coupled ultrasonic technology was proposed. It has lots of advantages, such as no contact wear, non-destructive, non-immersion, etc., so that it is a harsh environment to detect material performance that has a unique advantage. Wang *et al.* [23] applied the ultrasound delay time spectrum method for evaluating the interfacial bonding, results showed that the delay time peak of the weak bonding interface is much greater than that of the perfect interface. Chimenti [24] introduced the application of air-coupled ultrasound in material performance testing. Lamb waves was utilized to measure the properties of elastic or viscoelastic materials. Li *et al.* [25] established a model of air-coupled ultrasonic guided waves in a two-layered slab medium and proposed a layered defect detection method based on the wavelet energy value to realize defect quantitative analysis for non-metallic anticorrosion coatings. Sankar *et al.* [26] put forward a rapid and non-contact inspection technique for a composite structural component using ultrasonic guided waves. The correlation between the numerically simulated and experimentally obtained B-scans was established. Different regions in the B-scan images could be employed to locate and identify defects in the sample. Römmeler *et al.* [27] found that when the pipeline was scanned by a single-sided pitch captured device, the defect wound case a characteristic pattern in the collected data. The experimental results were verified by mathematical models, which proved the possibility of using air-coupled ultrasonic to detect defects in thin polymer plates. Fan *et al.* [28] established a multi-physics model to simulate the wave propagation at different incident angles. It is verified that this model could provide a convenient and accurate way using leaky Lamb waves of an air-coupled ultrasound. Based on the spring model and the potential function theory, Wang *et al.* [29] set up a model to predict the transmission spectrum in a double-layer adhesive structure. A method to optimize the measurement parameters, such as the incident angle and center frequency, was put forward to analyze the relationship between the resonant peaks and the interface stiffness at the frequency lower than 1MHz.

However, only a few scholars have applied air-coupled ultrasound to the quality inspection of bonded structures. There is a lack of exploration between the acoustic parameters and the interface quality of bonded structures. In this paper, a mathematical model is established by the propagation mechanism of the air-coupled transmission longitudinal waves in the bonded structure. Taking polymethyl methacrylate (PMMA) and aluminum (Al) as tested the double-layer bonded plate, the propagation characteristics of the air-coupled ultrasound in it are discussed. The correlation among the resonant frequency, the transmission coefficient and the interface stiffness can be obtained by numerical simulation analysis. An air-coupled ultrasonic experiment

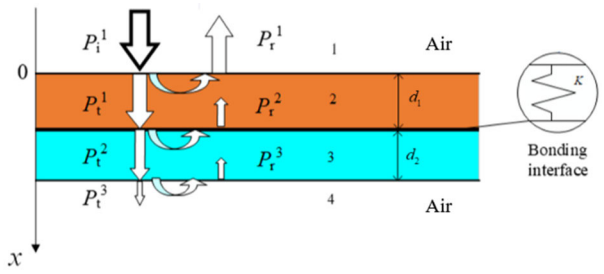

FIGURE 1. The schematic diagram of ultrasonic propagation in a double-layered bonded structure.

is implemented to verify the validity of the calculation results.

II. ULTRASOUND PROPAGATION CHARACTERISTICS IN DOUBLE-LAYER BONDED STRUCTURE

A. PHYSICAL MODEL

The schematic diagram of the air-coupled ultrasound propagated in the double-layer bonded structure is illustrated in Fig. 1. To simplify physical model, the ultrasonic incident angle is selected to be nil. With the incidence of the plane longitudinal wave P_{i}^1, a portion of the energy is reflected (shown as P_{r}^1 in Fig. 1), while the rest of the energy is transmitted into the bonding medium 2 and medium 3. Ultrasonic longitudinal waves are incident perpendicularly from medium 1, through medium 2 and medium 3, and finally transmits into medium 4. Reflection and transmission occur at the interface of different media. Medium1 and medium 4 are air. Medium 2 and medium 3 are measured double-layer bonded plate. $P_{\mathrm{i}}^{\mathrm{n}}$, $\mathrm{P}_{\mathrm{r}}^{\mathrm{n}}$, and $P_{\mathrm{t}}^{\mathrm{n}}$ $(n = 1, 2, 3)$ represent the amplitudes of the incident, reflected, and transmitted sound pressure, respectively. The superscript n denotes the corresponding medium. The transmitted wave in the upper layer of the interface is the incident wave of the lower, therefor, $P_{\mathrm{t}}^1 = \mathrm{P}_{\mathrm{i}}^2$, $P_{\mathrm{t}}^2 = P_{\mathrm{i}}^3$, $P_{\mathrm{t}}^3 = P_{\mathrm{i}}^4$. d_1 and d_2 are the thickness of medium 2 and medium 3, respectively.

The bonding interface is treated as a spring model, and K denotes the stiffness coefficient of double layers. The thickness of the bonding interface is ignored because it is small enough. There is no wave mode conversion for normal incidence of sound waves. Stiffness coefficients affecting the propagation characteristics of the sound wave are only the normal stiffness coefficient of the interface, which refers to the normal stiffness coefficient in this paper. Assume that the vertical direction down is positive, the interface of the medium 1 and medium 2 is $x = 0$.

B. MATHEMATICAL MODEL

Spring model was adopted to simulate interface stiffness [23]. A local coordinate system is introduced in each layer, and the position where the sound waves enter the interface of the layer is set as the origin of coordinates. The wave propagation law of multilayers is usually studied by means of transfer matrix, which is suitable for the transmission of sound waves in infinite laminates. However, when the sound wave is in a high frequency or the thickness of the plates is too large, the high frequency overflow will occur. In order to solve this problem, the whole matrix method is used to establish the mathematical model, which can avoid the overflow phenomenon [30]. The formula of linear sound wave is

$$\frac{\partial^2 P}{\partial x^2} = \frac{1}{c^2}\frac{\partial^2 P}{\partial t^2} \tag{1}$$

where, P is the sound pressure, and c is the wave velocity. According to the relationship between sound pressure and particle vibration velocity [31], P_{n} $(P_{\mathrm{n}} = P_{\mathrm{i}}^{\mathrm{n}} + P_{\mathrm{r}}^{\mathrm{n}})$ can be expressed as follows:

$$\begin{aligned} P_1 &= E(P_i^1 e^{-jk_1 x} + P_r^1 e^{jk_1 x}) \\ P_2 &= E(P_t^1 e^{-jk_2 x} + P_r^2 e^{jk_2 x}) \\ P_3 &= E(P_t^2 e^{-jk_3 x} + P_r^3 e^{jk_3 x}) \\ P_4 &= E(P_t^3 e^{-jk_4 x}) \end{aligned} \tag{2}$$

According to the knowledge in material mechanics [32], the longitudinal wave velocity c_{L} and transverse wave velocity c_{S} of solids have the following relationship with the Lamé constants (λ, μ) and the medium density ρ:

$$\rho c_L^2 = \lambda + 2\mu, \quad \rho c_S^2 = \mu \tag{3}$$

The particle velocity of each layer V_{n} $(n = 1, 2, 3, 4)$ can be calculated as follows on the basis of formula (2) and (3):

$$\begin{aligned} V_1 &= \left(\frac{E}{z_1}\right)\left(P_i^1 e^{-jk_1 x} - P_r^1 e^{jk_1 x}\right) \\ V_2 &= \left(\frac{E}{z_2}\right)\left(P_t^1 e^{-jk_2 x} - P_r^2 e^{jk_2 x}\right) \\ V_3 &= \left(\frac{E}{z_3}\right)\left(P_{\mathrm{t}}^2 e^{-jk_3 x} - P_r^3 e^{jk_3 x}\right) \\ V_4 &= \left(\frac{E}{z_4}\right) P_t^3 e^{-jk_4 x} \end{aligned} \tag{4}$$

where, $E = e^{j\omega t}$ is a time dependent on factor; Z_n $(Z_n = \rho_n c_n)$ is the acoustic impedance of the medium that is determined by the density of the medium (ρ_n) and the longitudinal wave sound speed in the medium (c_n) $(n = 1,2,3,4)$; $k_n = \omega/c_n$ is the wave number reflecting the density of the wave in space. That is, the number of waves in the length of 2π, $\omega = 2\,\pi f$ is the circular frequency that reflects the flux of the wave, refers to the number of waves passing in 2π seconds at a certain point in space, where, f is frequency of the ultrasonic wave. Let $P_i^2/P_i^1 = N_2$, $P_r^2/P_i^1 = M_2$, $P_i^3/P_i^1 = N_3$, $P_r^3/P_i^1 = M_3$, the reflection coefficient $R = P_r^1/P_i^1$, and the transmission coefficient $T = P_t^3/P_i^1$. The spring model is utilized to simulate the bonding interface. In this case, the boundary conditions are that Sound pressure and particle vibration speed are continuous at the interface. It can be represented as:

$$\begin{aligned} &P_1 = P_2, V_1 = V_2|_{x=0} \\ &P_2 = P_3, \frac{\partial P_2}{\partial t} = K\,(V_2 - V_3)|_{x=d_1} \\ &P_3 = P_4, V_3 = V_4|_{x=d_2} \end{aligned} \tag{5}$$

TABLE 1. Physical parameters of materials.

Materials	Longitudinal wave velocity /(m/s)	Density /(kg/m^3)	Acoustic impedance/Rayl
Air	343	1.29	442.47
PMMA	2700	1180	2.86×10^6
Al	6320	2770	16.54×10^6

By substituting formulas (2) and (4) into formula (5), the follow formula can be obtained:

$$\begin{aligned}
P_i^1 + P_r^1 - P_i^2 - P_r^2 &= 0|_{z=0} \\
\left(P_i^1 - P_r^1\right)\frac{1}{z_1} - \frac{1}{z_2}\left(P_i^2 - P_r^2\right) &= 0|_{z=0} \\
P_i^2 e^{-ik_2d_1} + P_r^2 e^{ik_2d_1} - P_i^3 - P_r^3 &= 0|_{z=d_1} \\
P_i^2 e^{-ik_2d_1}\left(\mathrm{i}\omega - \frac{K}{z_2}\right) + P_r^2 e^{ik_2d_1}\left(\mathrm{i}\omega + \frac{K}{z_2}\right) + \frac{K}{z_3}P_i^3 - \frac{K}{z_3}P_r^3 & \\
= 0|_{z=d_1} & \\
P_i^3 e^{-ik_3d_2} + P_r^3 e^{ik_3d_2} - P_t^3 &= 0|_{z=d_2} \\
P_i^3\frac{e^{-ik_3d_2}}{z_3} + P_r^3\frac{e^{ik_3d_2}}{z_3} - P_{\mathrm{t}}^3\frac{1}{z_4} &= 0|_{z=d_2}
\end{aligned} \tag{6}$$

As mentioned previously, there are four layers in Fig. 1, and a bonded structure is composed of the second layer, third layer and their interface. According to the formula (6), using the global matrix as follows:

It is 6 × 6 matrix in above formula, the odd rows are derived from the sound pressure, while the even rows are obtained from the particle velocity. The transmission coefficient T from ultrasonic waves in the measured medium can be calculated by solving the formula (7).

III. ANALYTICAL SIMULATION RESULT

Solution the formula (7) of the previous chapter using numerical simulation. The material of medium 2 is PMMA and that of medium 3 is Al. The thicknesses of PMMA plate (d_1) are 1mm, 3mm, 5mm, respectively, and the thickness of Al plate (d_2) is 1mm. The physical parameters of materials are shown in Tab. 1.

Fig. 2 illustrates the frequency spectrum characteristics of PMMA with a thickness 3mm and Al with a thickness 1 mm in different stiffness coefficients, where the

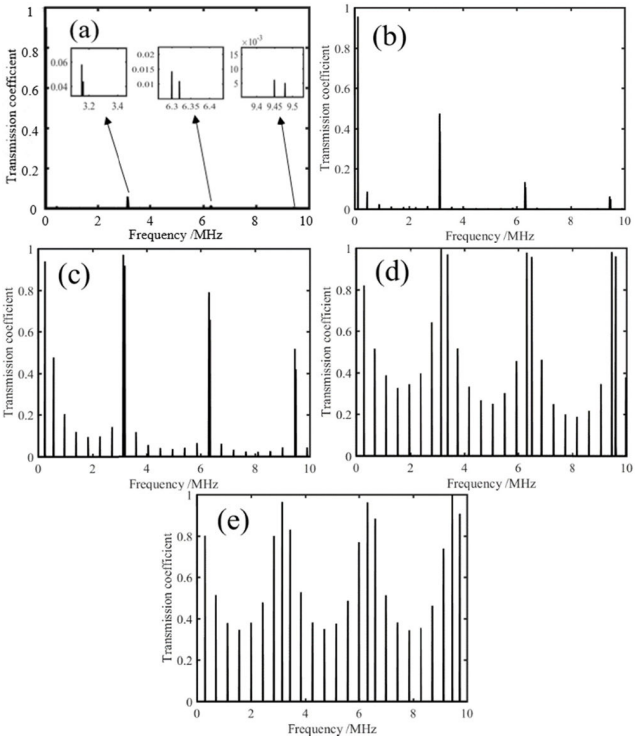

FIGURE 2. Transmission frequency spectrum under different stiffness coefficients (d_1 = 3mm, d_2 = 1mm) (a) K = 1e11N·m^{-3}, (b) K = 1e12N·m^{-3}, (c) K = 1e13N·m^{-3}, (d) K = 1e14N·m^{-3}, (e) K = 1e15N·m^{-3}.

stiffness coefficients are K = 1e11N·m^{-3}, K = 1e12N·m^{-3}, K = 1e13 N·m^{-3}, K = 1e14N·m^{-3}, K = 1e15N·m^{-3}, respectively. As observed in Figure 2, there are two type resonance frequencies. It should be explained that the resonance frequency refers to the frequency corresponding to the transmission coefficient peak. The first type resonance frequency (RFI) has a smaller the transmission coefficient peak, and its interval is about 0.45MHz. The transmission coefficient peak of second type resonance frequency (RFII) is relatively larger, and the frequency interval is about 3.19MHz. At the same time, the transmission coefficient peaks from the RFII are greater than these of the RFI, and the former has a local maximum. As a result, it shows a ''periodicity'' in the figure, which is a uniform frequency interval. The RFI interval is related to the thickness of the first layer (PMMA), and the

$$\begin{bmatrix}
1 & -1 & -1 & 0 & 0 & 0 \\
\frac{1}{z_1} & \frac{1}{z_2} & \frac{-1}{z_2} & 0 & 0 & 0 \\
0 & e^{-jk_2d_1} & e^{jk_2d_1} & -1 & -1 & 0 \\
0 & \left(j\omega - \frac{K}{z_2}\right)e^{-jk_2d_1} & \left(j\omega + \frac{K}{z_2}\right)e^{jk_2d_1} & \frac{K}{z_3} & \frac{-K}{z_3} & 0 \\
0 & 0 & 0 & e^{-jk_3d_2} & e^{jk_3d_2} & -1 \\
0 & 0 & 0 & \frac{e^{-jk_3d_2}}{z_3} & \frac{-e^{jk_3d_2}}{z_3} & \frac{-1}{z_4}
\end{bmatrix}
\begin{bmatrix} R \\ N_2 \\ M_2 \\ N_3 \\ M_3 \\ T \end{bmatrix}
=
\begin{bmatrix} -1 \\ \frac{1}{z_1} \\ 0 \\ 0 \\ 0 \\ 0 \end{bmatrix} \tag{7}$$

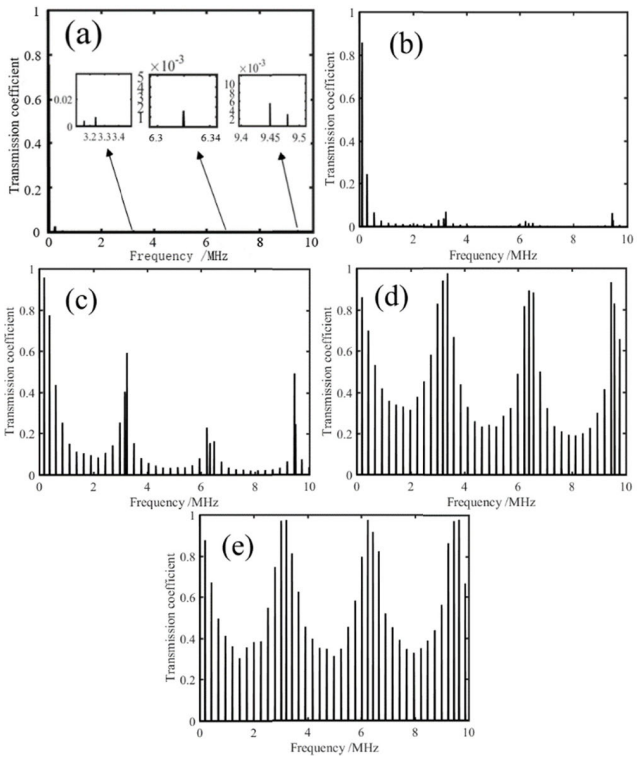

FIGURE 3. Transmission frequency spectrum under different stiffness coefficients ($d_1 = 5$mm, $d_2 = 1$mm) (a) $K = 1e11N{\cdot}m^{-3}$, (b) $K = 1e12N{\cdot}m^{-3}$, (c) $K = 1e13N{\cdot}m^{-3}$, (d) $K = 1e14N{\cdot}m^{-3}$, (e) $K = 1e15N{\cdot}m^{-3}$.

RFI changes with the increase of the stiffness coefficient. The RFII interval is associated with the thickness of the second layer (Al). However, the RFII is independent of the stiffness coefficient. The specific relationship among the stiffness coefficient, the RFI and the RFII will be given in the following analysis respectively.

The frequency spectrum characteristics under different stiffness coefficients for PMMA with thickness 5 mm and Al with thickness 1mm in Fig.3. The change rule of frequency spectrum from the Fig. 3 is similar with the Fig. 2. however, there are the more the number and the smaller interval from RFI due to thickness of PMMA from 3mm to 5mm, which is about 0.26MHz. The thickness of the second layer (Al) does not change, so the interval of the RFII is still about 3.22MHz. Further work has to be undertaken in order to explain in more details the dependence of the RFI interval and the thickness of the first layer PMMA. The relationship between the transmission coefficient and frequency is presented in Fig. 4. the RFI interval is about 1.31MHz with 1mm thickness PMMA and 1mm thickness Al in Fig. 4(a). Similarly, the RFI interval is about 0.45MHz with 3mm thickness PMMA and 1mm thickness Al in Fig. 4(b), and the RFI interval is about 0.27 MHz with 5mm thickness PMMA and 1mm thickness Al in Fig. 4(c). Thus, the thicker the PMMA layer, the smaller the RFI interval. However, the thickness of Al is always 1mm, which has not changed, and the RFII interval is still 3.20MHz. The transmission coefficient increases with the increase of the stiffness coefficient from Fig. 4. It is shown that the stiffness coefficient from $1e11N{\cdot}m^{-3}$ to $1e13N{\cdot}m^{-3}$ has an obvious increasing, but which becomes smaller from $1e14N{\cdot}m^{-3}$ to $1e15N{\cdot}m^{-3}$. When the stiffness coefficient continues to increase (more than $1e15N{\cdot}m^{-3}$), the transmission coefficient approached to a unchangeability. The change of stiffness coefficient represents the change process from weak bonding interface to rigid bonding interface.

Furthermore, the relevance of the RFI and RFII interval and the thickness of the upper and lower layers is shown in Fig. 5, which is satisfied formula $c_L = 2f_0d$, where c_L is the longitudinal wave velocity, f_0 is the resonance frequency interval, d is the thickness. The velocity of longitudinal wave in PMMA is about 2603m/s by fitting, which is very close to 2700m/s given in Tab. 1. In addition, the thickness of the Al layer is 1mm, and the RFII interval is about 3.20MHz. The sound velocity in Al layer by calculated is about 6400m/s, which is also very close to 6320m/s given in Tab.1. Therefore, the simulation results are correct from the above thickness testing.

Fig. 6 illustrates the resonant frequency, including the RFI and the RFII, depends on the stiffness coefficient, where, Fig. 6(a)-6(c) present relevance of two parameters in three section (0-3MHz, 3-6 MHz and 6-10 MHz) for more clarity and convenience, respectively. As mentioned above, the RFI from before seven peaks is related to the thickness of the first layer PMMA. With the increase of stiffness coefficient, the

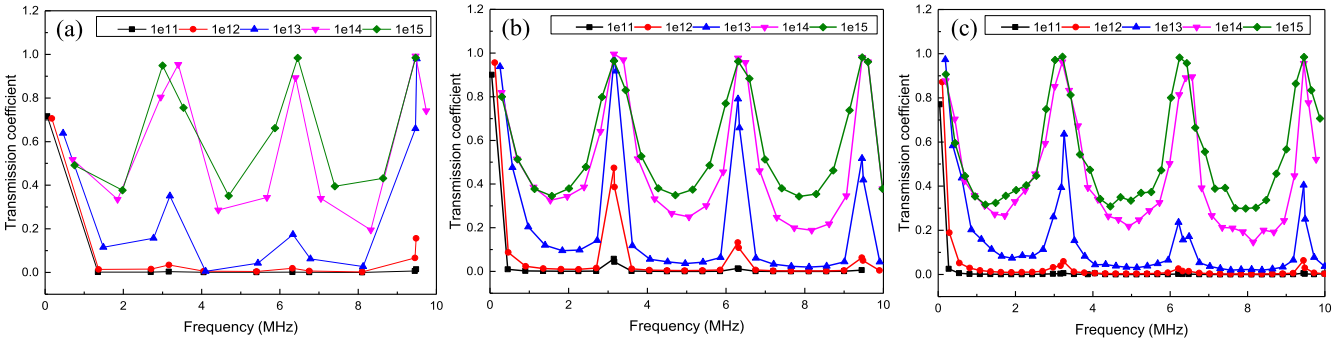

FIGURE 4. Transmission frequency spectrum under different thickness(a) $d_1 = 1$mm, $d_2 = 1$mm, (b) $d_1 = 3$mm, $d_2 = 1$mm, (c) $d_1 = 5$mm, $d_2 = 1$mm.

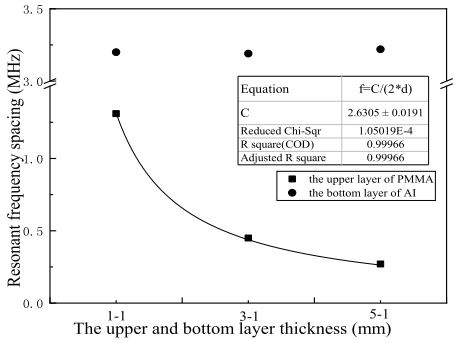

FIGURE 5. Relationship between resonant frequency (the RFI and RFII) and PMMA and Al layer thickness.

RFI increases in Fig.6. Nevertheless, the trend of transmission coefficient peak from the RFI to the right are different, which from the RFI change obviously. The more the number peak of the RFI, right shift is not obvious. For peak number 8, belong to the RFII, the frequency shift doesn't change with the increase of the stiffness coefficient. The variation rule from Fig. 6(b) are similar with Fig. 6(c). Fig. 7 can be obtained by calculating the resonant frequency shift distance of each peak in Fig. 6. With the increase of the number of transmission coefficient peaks, the resonant frequency shifts distance decreases, and right shift of the RFII, from peak number 8 is close to 0.

To sum up, with the increase of the stiffness coefficient, the RFI all moves to the right. When it reaches the RFII, there will be a cutoff frequency. A similar law emerges within each ''period'' of the RFII.

IV. AIR-COUPLED ULTRASONIC EXPERIMENT

A. EXPERIMENTAL MATERIALS

An experimental material is the same as the simulation choice. The PMMA with model MR-200 made by Japan Mitsubishi Group and Al with model 1060 produced in China is selected. The thicknesses of PMMA plate are 5mm and 10mm, respectively. the surface is a square with a length of 100mm. The thickness of Al plate is 1mm, and the surface is a square with a length of 65mm. The adhesive is epoxy resin AB glue (Component A is acrylic epoxy resin, and component B is modified amine, made by Jianhua Template Design Co.). The first air layer is the coupling medium, which is located between an air sensor and the upper of bonded structures. The last air layer is severed as the semi-infinite space. The change of interface stiffness is achieved by bonding time. The curing time of AB glue is 8-10 hours, consequently, the bonded plate was detected every other hour before bonding time reaches 10 hours. Only four representative bonding time results by ultrasonic experiment are given in this paper for simplicity (1 hour, 5 hours, 7 hours, and 10 hours).

B. EXPERIMENTAL DEVICE AND METHOD

The ultrasonic detection system is shown in Fig.8, where ① and ② are, respectively, the air-coupled ultrasonic transmitting sensor and receiving sensor. The height of sensors can be adjusted by moving in the guide ⑤. To increase the energy of transmitted sound waves and ensure the accuracy of the results, the two sensors must be directly opposite and the central axis should be collinear. ④ is the tested double-layer bonded plate, which is clamped and fixed by the U-shaped retaining clip ③. The U-shaped fixture is fixed on a rotating table. The incidence angle of the sensor can be adjusted by rotating in the rotary table. There is a scale mark that displays the angle reading of incidence in the rotary table. It is necessary to make the bonded plate in a vertical position before adjusting the incident angle of the sensor. ⑥ is an amplifier, which has two roles, amplifying the received signal (the amplification is 60 dB) and filtering clutter. ⑦ is an ultrasonic pulser/receiver device. ⑧ is a personal computer, which can be used to control the ultrasonic device to excite ultrasound and record the experimental data.

The ultrasonic device is produced by Japan Probe Company (model JPR-10CN), which has good stability in the data acquisition process and can integrate ultrasonic transmitting/receiving and A/D conversion function. The sampling frequency is set to 10MHz. The air-coupled sensors (model 0.8K14 × 20N-RX, made by Japan Probe company) with a center frequency of 0.8 MHz were applied. The ultrasonic pulses generated from the transmitting sensor, propagating through the air and the measured bonded plates and finally are received by the receiving sensor. The signal is amplified by the amplifier and then converted into the computer through the A/D acquisition card, which is analyzed and processed.

C. EXPERIMENTAL RESULTS AND ANALYSIS

In order to prove the above simulation results, it is necessary to measure the transmission coefficient in an air couple ultrasonic testing experiment. According to solution method of the transmission coefficient, the following formula can be used [31]

$$T = \frac{U(f)}{I(f)} \tag{8}$$

where $U(f)$ is the spectrum of the transmitted signal and $I(f)$ is the spectrum of the incident signal. The received signal, there is no sample to be placed between the two sensors, is taken as referent. Fig.9 (a) is the received signal (referent). $I(f)$ is the normalized spectrum by FFT calculate from received signal, as shown in Fig. 9(b). As can be seen from Fig.9 (b), the frequency bandwidth of the air-coupled ultrasonic sensor is very narrow, which is from 0.7MHz to 0.8MHz, but it still has some reference significance in the 0.5MHz∼1MHz area. The frequency from 0.5MHz to 1MHz is selected as the final observation range.

Fig.10 presents the transmission spectrum from an ultrasonic experimental by FFT at different bonding times (1 hour, 5 hours, 7 hours, 10 hours). The different bonding time was used to simulate the change of stiffness coefficients. The frequency ranges from 0.5MHz to 1MHz is selected for

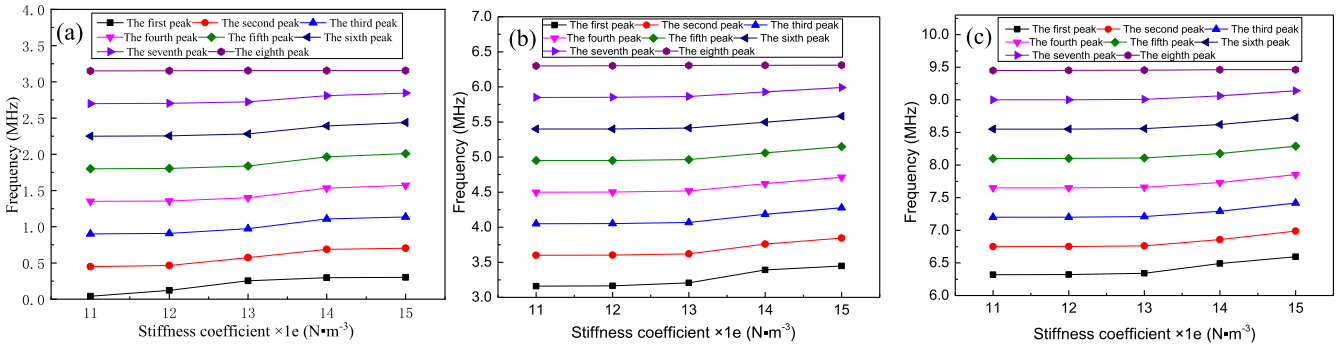

FIGURE 6. Relationship between resonant frequency (the RFI and RFII) and stiffness coefficient (a) 0-3 MHz (b) 3-6MHz (c) 6-10MHz.

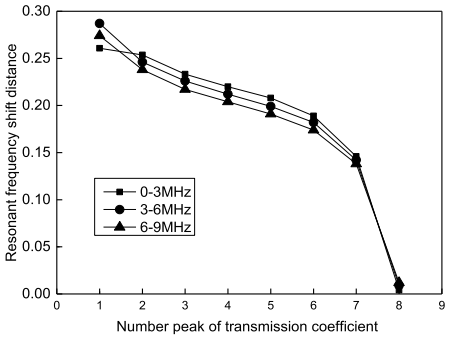

FIGURE 7. Resonant frequency shift distance.

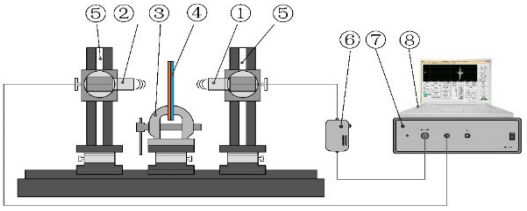

FIGURE 8. Ultrasonic experimental equipment for measuring the interfacial bonding characteristics of the double-layer structure. ① Transmitting sensor ② Receiving sensor ③ U-shaped fixture ④ Sample plate ⑤ Guide ⑥ Amplifier ⑦ Ultrasonic pulser/receiver device ⑧ PC.

analysis according to the above sensor bandwidth. Fig.10(a) and Fig.10(b) are 5mm and 10mm PMMA bonded with 1mm Al, respectively. There are three resonant frequency peaks in the range of 0.5MHz to 1MHz in Fig.10(a). Similarly, two resonant frequency peaks can be found as shown in Fig.10 (b). The highest resonant peak of the spectrum is located at the frequency of 0.7MHz-0.75MHz. The center frequency is shifted due to test samples. Each transmission peak from Fig.10 (a) and Fig.10 (b) included the transmission coefficient. The RFI and its interval were recorded in Tab.2 and Tab.3, respectively.

From the part 3 analytical simulation result, the RFI interval increases twice when d_1 reduces to half, and it seems to occur the same phenomenon in Fig.10. The RFI interval (0.268 MHz) of 5mm PMMA bonded with 1mm Al is almost twice that (0.145 MHz) of 10mm PMMA bonded with 1mm Al from Tab. 2 and Tab. 3. The measured thickness and error can be calculated according to the RFI interval as shown in

TABLE 2. Resonant frequency and transmission coefficient of the resonant peak at different bonding times (10mm PMMA-1mm Al).

Transmission peak		Bonding for 1 hour	Bonding for 5 hours	Bonding for 7 hours	Bonding for 10 hours
The first peak	RFI (MHz)	0.616	0.63	0.633	0.635
	Transmission coefficient	0.1031	0.1556	0.1635	0.164
The second peak	RFI (MHz)	0.745	0.766	0.767	0.769
	Transmission coefficient	0.5008	0.8156	0.8666	0.8954
The third peak	RFI (MHz)	0.907	0.905	0.915	0.909
	Transmission coefficient	0.0285	0.0721	0.036	0.048
RFI interval (MHz)		0.1455	0.136	0.141	0.137

TABLE 3. Resonant frequency and transmission coefficient of the resonant peak at different bonding times (5mm PMMA-1mm Al).

Transmission peak		Bonding for 1 hour	Bonding for 5 hours	Bonding for 7 hours	Bonding for 10 hours
The first peak	RFI (MHz)	0.69	0.693	0.695	0.696
	Transmission coefficient	0.479	0.5838	0.746	0.9174
The second peak	RFI (MHz)	0.958	0.959	0.96	0.973
	Transmission coefficient	0.0774	0.1218	0.1559	0.1799
RFI interval (MHz)		0.268	0.266	0.265	0.277

TABLE 4. Measured thickness and its error at different bonding times.

Bonding time/hours	Theoretical thickness d_1=5mm		Theoretical thickness d_1=10mm	
	Measured thickness d/mm($d=c_L/(2f_0)$)	error (%)	Measured thickness d/mm($d=c_L/(2f_0)$)	error (%)
1	5.037	0.74%	9.278	7.22%
5	5.075	1.50%	9.926	0.74%
7	5.094	1.88%	9.574	4.26%
10	4.873	2.53%	9.854	1.46%

Tab. 4, where velocity of longitudinal wave in PMMA is 2700m/s as shown in Tab. 1. It is concluded that measured thicknesses are in good agreement with theoretical thicknesses. The maximum error is 7.22% from 10mm thickness PMMA with 1 hour time, and the others are less than 4.22%. Among of these errors, the minimum error is only 0.74%. As we all know, the signal near the center frequency is more accurate and reliable, so the second resonant frequency peak in Fig.10 (a) and the first resonant frequency peak in Fig.10 (b) are selected for analysis. The relationships among the resonant frequency, the transmission coefficient and the

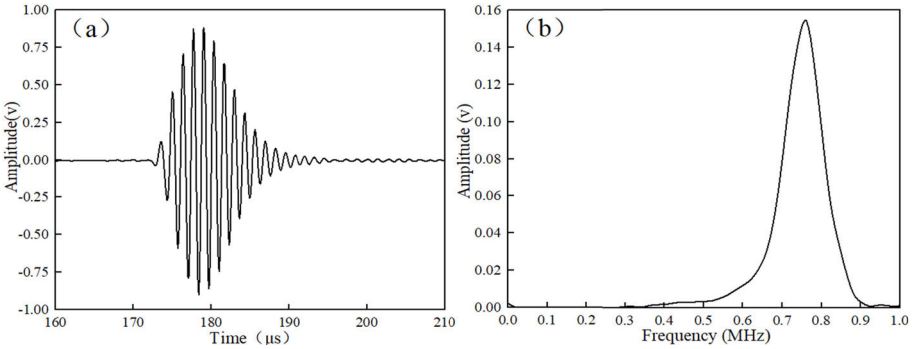

FIGURE 9. Reference signal: (a) waveform (b) frequency spectrum.

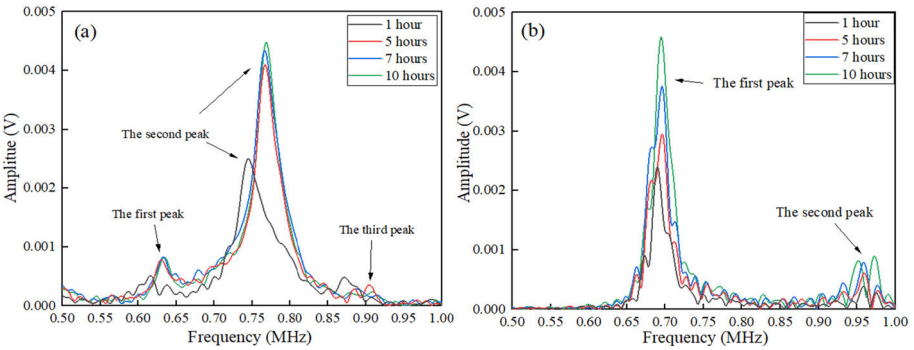

FIGURE 10. Ultrasonic transmission spectrum at different bonding time. (a) $d_1 = 10$mm, $d_2 = 1$mm (b) $d_1 = 5$mm, $d_2 = 1$mm.

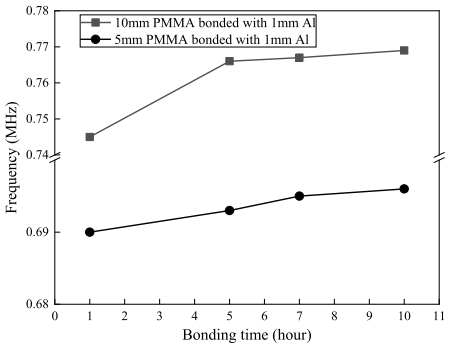

FIGURE 11. Correlation between the RFI and bonding time.

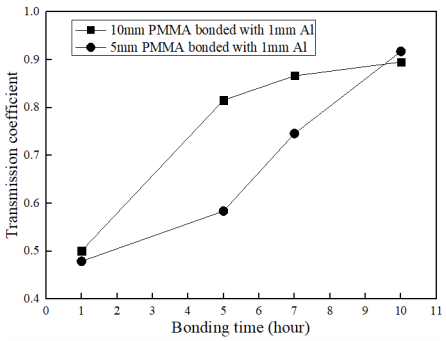

FIGURE 12. Relationship between the transmission coefficient and bonding time.

bonding time are pointed out in Fig.11 and Fig12. As illustrated in Fig.11, the RFI increases with the boning time turns longer, which drifts to high-frequency from 10mm PMMA bonded with 1mm Al and 5mm PMMA bonded with 1mm Al. This is in line with the ''peak drift'' phenomenon appearing in the simulation results. In additional, with the increase of bonding time, the transmission coefficient also emerges an increasing trend from Fig.12. This conclusion also well verifies the simulation results. By comparison with the sensitivity of the RFI to the stiffness coefficient, the transmission coefficient is more suitable to measure and evaluate the stiffness coefficient. In general, the stiffness coefficient can be judged by both the RFI and the transmission coefficient.

It should be noted there is no the RFII related to the second layer Al in Fig. 10. According to the numerical calculation results, the RFII from 1mm thickness of Al layer is about 3.2MHz. Because the center frequency of sensors in ultrasonic experiment is about 0.8 MHz and the bandwidth is insufficient. Only the transmission spectrum in the frequency range of 0.5 MHz-1.0 MHz is given.

V. CONCLUSION

The mathematic model, which describe interface quality of bonding structure, was deduced. By numerical solve, the correlation among the parameters, such as the stiffness coefficient, the transmission coefficient and resonant frequency,

was illustrated. An air coupled ultrasonic testing experiment was using to prove result from numerical simulating. Two type resonant frequencies appear in the transmission frequency spectrum, which are from mathematic model by the numerical simulating. The interval of the RFI is related to the thickness of PMMA layer. However, the interval of the RFII depends on the thickness of Al layer. Increasing thickness from the PMMA layer, the peak number of the RFI increases, and the interval of RFI decreases at the same time. With the increase of the stiffness coefficient, all the RFI moves to the right. When the RFI reaches the RFII, there will be a cut-off frequency. A similar phenomenon can be observed in each ''period'' of the RFII. By ultrasonic experiment, the RFI interval (0.268MHz) with thickness 5mm PMMA layer is almost twice that (0.145MHz) with thickness 10mm PMMA. Nevertheless, there is no the RFII due to center of sensor 0.8MHz and insufficient the bandwidth. The results show no difference between the air couple ultrasonic experiment and the numerical simulating.

REFERENCES

[1] R. Talebitooti, H. D. Gohari, and M. R. Zarastvand, ''Multi objective optimization of sound transmission across laminated composite cylindrical shell lined with porous core investigating non-dominated sorting genetic algorithm,'' *Aerosp. Sci. Technol.*, vol. 69, pp. 269–280, Oct. 2017.
[2] M. R. Zarastvand, M. Ghassabi, and R. Talebitooti, ''A review approach for sound propagation prediction of plate constructions,'' *Arch. Comput. Methods Eng.*, Aug. 2020, Art. no. 125316.
[3] M. R. Zarastvand, M. Ghassabi, and R. Talebitooti, ''Acoustic insulation characteristics of shell structures: A review,'' *Arch. Comput. Methods Eng.*, vol. 1, pp. 1–9, Dec. 2019.
[4] R. Talebitooti and M. R. Zarastvand, ''The effect of nature of porous material on diffuse field acoustic transmission of the sandwich aerospace composite doubly curved shell,'' *Aerosp. Sci. Technol.*, vol. 78, pp. 157–170, Jul. 2018.
[5] H. D. Gohari, ''Acoustic performance prediction of a multilayered finite cylinder equipped with porous foam media,'' *J. Vib. Control.*, vol. 26, nos. 11–12, 2020, Art. no. 107754631989002.
[6] C. A. Ai, ''Ultrasonic test theory and technology for multilayered bonding structure,'' *Beijing, China, Nat. Defense Ind.*, vol. 2014, pp. 184–298, May 2014.
[7] W.-L. Wu, X.-G. Wang, Z.-C. Huang, and N.-X. Wu, ''Measurements of the weak bonding interfacial stiffness by using air-coupled ultrasound,'' *AIP Adv.*, vol. 7, no. 12, Dec. 2017, Art. no. 125316.
[8] P. Dou, T. Wu, Z. Luo, Z. Peng, and T. Sarkodie-Gyan, ''The application of the principle of wave superposition in ultrasonic measurement of lubricant film thickness,'' *Measurement*, vol. 137, pp. 312–322, Apr. 2019.
[9] J. L. Rose, ''Ultrasonic waves in solids,'' *Science*, vol. 2005, pp. 32–42, May 1999.
[10] Y. J. Wang, ''Sound reflection from layered solid medium with rigid and slip interfaces,'' *Acta Acustica.*, vol. .17, no. 12, pp. 81–92, Mar. 1992.
[11] S. I. Rokhlin and Y. J. Wang, ''Analysis of boundary conditions for elastic wave interaction with an interface between two solids,'' *J. Acoust. Soc. Amer.*, vol. 89, no. 2, pp. 503–515, Feb. 1991.
[12] A. Xiao-Min, ''Low-frequency characteristic of ultrasound reflection spectrum from adhesively bonded aluminum plates,'' *Appl. Acoustics.*, vol. .28, no. 5, pp. 190–194, May 2009.
[13] S. Banerjee, ''Theoretical modeling of guided wave propagation in a sandwich plate subjected to transient surface excitations,'' *Int. J. Solids Struct.*, vol. .49, no. 9, pp. 3233–3241, Nov. 2012.
[14] M. Castaings, ''SH ultrasonic guided waves for the evaluation of interfacial adhesion,'' *Ultrasonics*, vol. .54, no. 16, pp. 1760–1775, Sep. 2014.
[15] C. H. Yew and X. W. Weng, ''Using ultrasonic SH waves to estimate the quality of adhesive bonds in plate structures,'' *J. Acoust. Soc. Amer.*, vol. .9, no. 6, pp. 174–179, Jun. 1987.
[16] K. Zhang, S. Li, and Z. Zhou, ''Detection of disbonds in multi-layer bonded structures using the laser ultrasonic pulse-echo mode,'' *Ultrasonics*, vol. 94, pp. 411–418, Apr. 2019.
[17] F. Gao, L. Zeng, J. Lin, and Y. Shao, ''Damage assessment in composite laminates via broadband Lamb wave,'' *Ultrasonics*, vol. 86, pp. 49–58, May 2018.
[18] L. Liu, Y. Yang, Y. Pan, and Z. Zhong, ''The study of wave propagation in the air-coupled composite laminate,'' *Chin. J. Solid Mech.*, vol. .35, no. 7, pp. 8–14, Feb. 2014.
[19] J. Ding, B. Wu, and C. He, ''Reflection and transmission coefficients of the SH0 mode in the adhesive structures with imperfect interface,'' *Ultrasonics*, vol. 70, pp. 248–257, Aug. 2016.
[20] J. Liu, W. J. Xu, and W. X. Hu, ''Evolution of the ultrasonic resonance modes in a three-layer structure with change of material and interface adhesion properties,'' *Acta Phys. Sin.*, vol. .65, no. 13, pp. 228–240, Aug. 2016.
[21] D. W. Schindel, ''Air-coupled ultrasonic measurements of adhesively bonded multi-layer structures,'' *Ultrasonics*, vol. 37, no. 3, pp. 185–200, Mar. 1999.
[22] E. Blomme, D. Bulcaen, and F. Declercq, ''Air-coupled ultrasonic NDE: Experiments in the frequency range 750 kHz–2MHz,'' *NDT E Int.*, vol. 35, no. 7, pp. 417–426, Oct. 2002.
[23] X. Wang, L. Yao, Z. Huang, C. Ma, L. Zhang, and N. Wu, ''Evaluating interfacial bonding characteristics of the composite material thin layer by ultrasound delay time spectrum,'' *Compos. Struct.*, vol. .222, no. 9, pp. 1–8, Apr. 2019.
[24] D. E. Chimenti, ''Review of air-coupled ultrasonic materials characterization,'' *Ultrasonics*, vol. 54, no. 7, pp. 1804–1816, Sep. 2014.
[25] M. D. Li, ''Detection on delamination damage of nonmetallic erosion resistant coating based on ultrasonic guided waves,'' *China Test.*, vol. 44, no. 6, pp. 22–27, Jun. 2018.
[26] R. S. Panda, P. Rajagopal, and K. Balasubramaniam, ''Rapid guided wave inspection of complex stiffened composite structural components using non-contact air-coupled ultrasound,'' *Composite Struct.*, vol. 206, pp. 247–260, Dec. 2018.
[27] A. Römmeler, R. Furrer, U. Sennhauser, B. Lábke, J. Wermelinger, A. de Agostini, J. Dual, P. Zolliker, and J. Neuenschwander, ''Air coupled ultrasonic defect detection in polymer pipes,'' *NDT E Int.*, vol. 102, pp. 244–253, Mar. 2019.
[28] Z. Fan, W. Jiang, M. Cai, and W. M. D. Wright, ''The effects of air gap reflections during air-coupled leaky Lamb wave inspection of thin plates,'' *Ultrasonics*, vol. 65, pp. 282–295, Feb. 2016.
[29] X. G. Wang, W. L. Wu, Z. C. Huang, J. J. Chang, and N. X. Wu, ''Research on the transmission characteristics of air-coupled ultrasound in double-layered bonded structures,'' *Materials*, vol. .11, no. 14, pp. 1–13, Feb. 2018.
[30] X. G. Wang, ''Testing stiffness coefficient of coating interface based on ultrasonic numerical simulation,'' *Acta Mater. Compos. Sinica*, vol. .34, no. 6, pp. 1354–1359, Jun. 2014.
[31] D. Gonghuan, *Acoustical Foundations*. Nanjing, China: Nanjing Univ., 2012, pp. 107–152.
[32] S. Zhang, *Material Mechanics*. Beijing, China: Machinery Ind. Press., 2009, pp. 32–34.

XINGGUO WANG was born in Yichun, Heilongjiang, China, in 1980. He received the B.Sc. and M.Sc. degrees from Jiamusi University, in 2002 and 2005, respectively, and the Ph.D. degree from the Dalian University of Technology, in 2010. He is currently an Associate Professor with the Jingdezhen Ceramic Institute. He has authored/coauthored over 30 publications. His research interest includes ultrasonic testing.

JIAXIANG WANG was born in Xingren, Guizhou, China, in 1993. He is currently pursuing the master's degree in mechanical engineering with the Jingdezhen Ceramic Institute, Jingdezhen, China. His research interest includes ultrasonic testing.

ZHICHENG HUANG was born in Macheng, Hubei, China, in 1978. He received the B.Sc. and M.Sc. degrees from the Jingdezhen Ceramic Institute, in 2002 and 2005, respectively, and the Ph.D. degree from Tsinghua University, in 2016. He is currently an Associate Professor with the Jingdezhen Ceramic Institute. He has authored/coauthored over 20 publications. His research interest includes ultrasonic testing.

XIAOGAO LI was born in Nanchang, Jiangxi, China, in 1980. He received the Ph.D. degree from Southeast University, in 2020. He has published more than ten articles. His research interests include nonlinear system modeling and control, vehicle dynamics and control, advanced electric vehicle technology, and intelligent manufacturing technology.